

Robust Spectrum Management for DMT-Based Systems

Martin Wolkerstorfer, *Student Member, IEEE*, Driton Statovci, *Member, IEEE*, and Tomas Nordström, *Senior Member, IEEE*

Abstract—In recent years an increasing effort was made to reduce the energy consumption in digital subscriber line equipment. Dynamic spectrum management (DSM) has been identified as one promising method to achieve energy-efficiency in discrete multitone based systems. An open research question is how to ensure system robustness when applying highly optimized energy-efficient spectrum management. In this paper, we study the problem of uncertainty in crosstalk noise and parameters, the knowledge of which is indispensable for many DSM algorithms. We introduce robust optimization for spectrum balancing as a technique to achieve feasibility of the optimal power-allocation under a deterministic parameter uncertainty model. This can be seen as an extension of current schemes for spectrum balancing. As a special case we consider the simple strategy of scaling the crosstalk parameters to their worst-case values, which corresponds to a specific uncertainty model and entails no changes to current DSM algorithms. Finally, we quantify the benefit in worst-case performance and the price in terms of energy by simulations.

Index Terms—Optimization methods, resource management, robustness, subscriber loops.

I. INTRODUCTION

IN recent years, both companies and society have shown considerable interest in addressing the energy consumption of broadband access equipment, e.g., in digital subscriber lines (DSL) [1], [2]. Applied to discrete multitone (DMT) based systems, dynamic spectrum management (DSM) has been shown to be a candidate tool for this purpose [3]–[5]. Its effectiveness is fundamentally based on the existing relation between transmit power and system energy consumption in current DSL transceivers. However, the transmission at minimum energy may come at the expense of system robustness. It is therefore imperative to take robustness against model inaccuracies or unstable environments explicitly into account during the optimization process. The latter can be incorporated by an adequate noise margin, optimization of outage probabilities [6], and repeated optimization triggered for instance by changes detected in the environment. While uncertainty in the noise environment has previously been considered for improving DSM algorithms [6], it is the uncertainty in crosstalk

coefficients we are concerned with herein. The latter is also not directly tackled by the virtual noise concept [7], which is used in practice to compensate for uncertainty in crosstalk noise. Coefficient uncertainty may include estimation errors as well as implementation errors of the calculated power levels. Even when the possible estimation error can be made diminishingly small, especially the estimation of cross-channel information comes at the cost of time, bandwidth and energy. Note that our approach can easily be extended to additionally take uncertainties of the noise-power on each carrier and line into account.

While stochastic optimization uses a probabilistic description of uncertainties in objective and constraints, *robust optimization* uses a set-based approach to take errors of model parameters into account [8], [9], [10, Sec. 6.4]. Specific examples of how this approach has been applied to problems in communications can be found in [11]–[13]. We argue that DSL network operators are less interested in a probabilistic constraint of not meeting the imposed target-rates (i.e., an outage probability constraint) than in a guaranteed minimum rate. Currently bit-rates are fixed by the operators according to a service level agreement. Therefore, the feasibility of the operating point under minimum energy consumption should be the aim, where a given uncertainty model is anticipated. Differently stated, we are not concerned with a long-term performance observation as it is natural for instance when considering variations of wireless channels [14], but we expect the optimized power-allocation to be *worst-case robust*, i.e., robust under the worst parameters for the considered degree of model errors.

In this paper we will compare the worst-case rate-loss of the optimal *nominal* (i.e., nonrobust) bit-allocation to the price of the additional robustness in terms of power consumption. In [8] a similar comparison was done to show the effect of model-uncertainty in numerous standard linear programs. The behavior of our robust optimization approach and hence the comparison depends on the definition of a parameter uncertainty set. Therefore, we will explore two different uncertainty regions in the shape of a box and an ellipsoid, respectively, based on their representativeness and analytical/computational tractability. The former model corresponds to the simple idea of scaling crosstalk parameters to their worst-case values, the implementation of which involves no changes to current DSM schemes. As a pivotal point in this respect we will investigate the interrelation between the robust per-carrier power-allocation problems and the problem of allocating bits to carriers.

Our analysis is based on the hypothesis that the price of robust power-allocation in terms of additional energy consumption is lowered when applied in combination with bit-allocation over carriers, as the latter allows to assign heavily interfering users to different carriers. Based on the same argument, it is expected

Manuscript received February 26, 2009; accepted January 29, 2010. Date of publication March 11, 2010; date of current version May 14, 2010. The associate editor coordinating the review of this paper and approving it for publication was Prof. Amir Leshem. This work has been supported in part by the Austrian Government and the City of Vienna within the competence center program COMET.

The authors are with the Telecommunications Research Center Vienna (FTW), Donau-City-Straße 1, A-1220 Vienna, Austria (e-mail: wolkerstorfer@ftw.at; statovci@ftw.at; nordstrom@ftw.at).

Color versions of one or more of the figures in this paper are available online at <http://ieeexplore.ieee.org>.

Digital Object Identifier 10.1109/TSP.2010.2044291

that the additional energy consumption for robustness may not substantially depend on the specific shape of the uncertainty region but mainly on the level of robustness. In this study, we will explore to which extent and under which conditions these intuitions hold. Our main contributions are hence the quantification of the energy-cost of robust optimization in DSM based DSL systems for various levels of uncertainty, and the investigation of the impact of uncertainty-set shape on the complexity of DSM algorithms and the total spent energy for robust transmission.

This paper is composed of three parts. First, in Sections II and III, we present our system model and formulate the global primal and dual energy minimization problems as well as the subproblem of computing feasible per-carrier power-allocations. Second, in Section IV we derive the theoretical background to our main results on what we term *robust DSM*, being an approach to achieve worst-case optimality for deterministic parameter uncertainty in DMT based DSL systems. Emphasizing the differences between the two considered shapes of uncertainty regions from an optimization point of view, we derive outage probability bounds and feasibility conditions for the *per-carrier* power-allocation subproblem. Finally, the third part consists of Sections IV-D–IV-F and our simulations in Section V, where we study the impact of robust optimization on the multicarrier system as a whole, for instance by analyzing the sensitivity w.r.t. uncertainty parameters. Furthermore, we present how robust optimization can be applied in current spectrum balancing algorithms, at which additional complexity, and at which cost in terms of additional energy consumption. Finally, in Section VI we summarize this work and highlight our conclusions on the applicability of the proposed robust optimization approaches.

II. SYSTEM MODEL

We adopt the system model from [15] wherein a multiuser DSL network was considered with spectral cooperation among U active or inactive lines being under the control of our algorithm. The crosstalk noise introduced by these subscriber lines is regarded solely as noise by the receivers. A popular modulation scheme employed for the frequency selective DSL channel is discrete multitone (DMT), which under perfect synchronization among transceivers separates the channel into C orthogonal subchannels. Without loss of generality we assume that all U users deploy DMT modulation with the same number of carriers C . Furthermore, we assume a perfect duplexing scheme and therefore neglect near-end crosstalk. As the background noise at the receiver is typically low compared to the far-end crosstalk, the latter is the limiting factor for system performance. Under the mentioned conditions the achievable rate per complex modulated DMT-symbol for user $u \in \mathcal{U}$ on carrier $c \in \mathcal{C}$ can therefore be computed as

$$r_u^c(\mathbf{p}^c) = \log_2 \left(1 + \frac{p_u^c}{\Gamma((\mathbf{p}^c)^T \mathbf{G}_u^c + N_u^c)} \right) \quad (1)$$

where $\mathcal{U} = \{1, \dots, U\}$, $\mathcal{C} = \{1, \dots, C\}$, Γ models the SNR-gap to capacity, $\mathbf{p}^c = [p_1^c, \dots, p_U^c]^T$, and p_u^c is the power spectral density (PSD) allocated on carrier c by user u . Furthermore, we write $\mathbf{G}_u^c = [G_{u1}^c, \dots, G_{uU}^c]^T$, with $G_{uu}^c = 0$ and G_{uv}^c and N_u^c denoting the squared magnitude of

the cross-channel transfer coefficient from user v to user u on carrier c and noise power density of user u on carrier c , respectively, where both are normalized by the squared magnitude of the direct channel transfer coefficient of user u .

III. GLOBAL PRIMAL AND DUAL PROBLEMS

Complementary to the power-constrained rate-maximization problem [16], the problem of optimizing energy-efficiency for multiuser DMT-based DSL networks with integer bit-allocation, in the following referred to as *primal nominal problem*, can be formulated as

$$\underset{\mathbf{p}, \mathbf{b}}{\text{minimize}} \quad \sum_{u \in \mathcal{U}} w_u \sum_{c \in \mathcal{C}} p_u^c \quad (2a)$$

$$\text{subject to} \quad \sum_{c \in \mathcal{C}} b_u^c \geq R_u, \quad \forall u \in \mathcal{U}, \quad (2b)$$

$$\log_2 \left(1 + \frac{p_u^c}{\Gamma((\mathbf{p}^c)^T \mathbf{G}_u^c + N_u^c)} \right) \geq b_u^c, \\ \forall u \in \mathcal{U}, \quad c \in \mathcal{C}, \quad (2c)$$

$$\mathbf{0} \preceq \mathbf{p} \preceq \bar{\mathbf{p}}, \quad (2d)$$

$$b_u^c \in \mathcal{B}_u^c, \quad \forall u \in \mathcal{U}, \quad c \in \mathcal{C} \quad (2e)$$

where $\mathcal{B}_u^c = \{0, 1, \dots, \bar{b}_u^c\}$ is the discrete set of feasible bit-allocations per user and carrier and the number of loadable bits is bounded by the bit-cap \bar{b}_u^c . Furthermore, $\mathbf{p} = [(\mathbf{p}_1)^T, \dots, (\mathbf{p}_U)^T]^T \in \mathcal{R}^{UC}$, where the power-allocation of user u is written as $\mathbf{p}_u = [p_u^1, \dots, p_u^C]^T$, $\forall u \in \mathcal{U}$, and $\mathbf{b} \in \mathcal{R}^{UC}$, being defined similarly to \mathbf{p} , represents the number of bits loaded on all carriers by all users. The problem further includes spectral mask limits $\bar{\mathbf{p}} \in \mathcal{R}_+^{UC}$ and weights $w_u > 0$, $\forall u \in \mathcal{U}$, $\sum_{u \in \mathcal{U}} w_u = 1$, which may be used to trace the boundary of a “power-region” [3] or to communicate link congestion information to the physical layer [17]. Finally, we consider quality-of-service constraints in terms of target-rates R_u in [bits/DMT-symbol].

By extracting the optimization over \mathbf{p}^c , $\forall c \in \mathcal{C}$, from (2) and disregarding the mask constraints for the time being, we write the single-carrier power-allocation problem as (cf. the power control problem [18], [19])

$$\underset{\mathbf{p}^c \succeq \mathbf{0}}{\text{minimize}} \quad \sum_{u \in \mathcal{U}} p_u^c \\ \text{subject to} \quad (\mathbf{I} - \mathbf{F}^c) \mathbf{p}^c \succeq \mathbf{n}^c \quad (3)$$

where $\mathbf{F}^c \in \mathcal{R}^{U \times U}$, $\forall c \in \mathcal{C}$,

$$\mathbf{F}_{uv}^c = \Gamma \gamma_{uv}^c G_{uv}^c \quad (4)$$

$$\mathbf{n}^c = [\Gamma \gamma_1^c N_1^c, \dots, \Gamma \gamma_U^c N_U^c]^T \quad (5)$$

and $\gamma_u^c = (2^{b_u^c} - 1)$ is the target-SINR of user u on carrier c . While the SINR is regarded constant by this single-carrier problem, we will later see how the spectrum balancing algorithm optimizes and determines the values b_u^c and hence γ_u^c , $\forall c \in \mathcal{C}$, $u \in \mathcal{U}$. The SINR-constraints in linear program (3) keep the objective from attaining the minimum it would obtain when neglecting the SINR-constraints, which due to $\mathbf{p}^c \succeq \mathbf{0}$ is 0. Hence, at optimum the constraints hold with equality and we

obtain, provided the problem is feasible, the unique [20] optimal solution $\mathbf{p}^{c,*}$ of (3) through (cf. also [10, Ex. 4.8])

$$\mathbf{p}^{c,*} = (\mathbf{I} - \mathbf{F}^c)^{-1} \mathbf{n}^c. \quad (6)$$

Note that in (3) and all forthcoming robust per-carrier power-allocation problems we omitted the weights \mathbf{w} as the SINR-constraints would still hold with equality at optimum, leaving $\mathbf{p}^{c,*}$, $c \in \mathcal{C}$, unchanged. It is well known [18], [19] that, assuming *nonzero* background noise, crosstalk couplings and SINR-targets, a solution (i.e., a power-allocation feasible w.r.t. SINR and positivity constraints) to (3) exists iff

$$\rho(\mathbf{F}^c) < 1 \quad (7)$$

where $\rho(\cdot)$ denotes the spectral radius or Perron–Frobenius eigenvalue.

The joint consideration of power and bit-allocation in (2) hence emphasizes the subproblem of computing a power-allocation on each carrier for a given bit-allocation as demanded by constraint (2c). While these variables are unambiguously coupled in this nominal problem by (6), later on we consider the problem of robust DSM and the application of ellipsoidal uncertainty regions. These on the other hand necessitate to solve per-carrier subproblems to map between bit-loadings and power-allocation, similar to the problem of robust power control. Hence, the distinction between power and bit-allocation will turn out useful to clarify the underlying power-allocation problem on the solution of which we will base our robust DSM algorithm, and to derive several corresponding feasibility conditions. For clarification of this distinction we will refer to a “bit-allocation” when considering the number of bits loaded per carrier as variables, while by “power-allocation” we refer to the problem of computing the power necessary to support a *fixed* number of bits (e.g., as assigned by a DSM algorithm).

Problem (2) consists of many per-carrier subproblems which are coupled by the users’ target-rate constraints. Since the left-hand side in (2b) is simply a sum, the problem is decomposable by the linear dual relaxation (cf. also the discussion in [15]). Relaxing only parts of the constraints in (2), its partial dual, which in the following will be referred to as the *dual nominal problem*, is given as

$$\begin{aligned} & \underset{\boldsymbol{\lambda}}{\text{maximize}} \quad \underset{\mathbf{p}, \mathbf{b}}{\text{minimize}} \quad \sum_{c \in \mathcal{C}} L^c(\mathbf{p}^c, \mathbf{b}^c, \boldsymbol{\lambda}) \\ & \text{subject to} \quad r_u^c(\mathbf{p}^c) \geq b_u^c, \quad \forall u \in \mathcal{U}, \quad c \in \mathcal{C}, \\ & \quad \mathbf{0} \preceq \mathbf{p} \preceq \bar{\mathbf{p}}, \quad \boldsymbol{\lambda} \geq \mathbf{0}, \\ & \quad b_u^c \in \mathcal{B}_u^c, \quad \forall u \in \mathcal{U}, \quad c \in \mathcal{C} \end{aligned} \quad (8)$$

where the objective (partial Lagrangian) is written as a sum of C per-carrier Lagrangians

$$L^c(\mathbf{p}^c, \mathbf{b}^c, \boldsymbol{\lambda}) = \sum_{u \in \mathcal{U}} w_u p_u^c + \sum_{u \in \mathcal{U}} \lambda_u \left(\frac{R_u}{C} - b_u^c \right). \quad (9)$$

We see that for fixed values of multipliers $\boldsymbol{\lambda} \in \mathcal{R}^U$ the per-carrier Lagrangians can be minimized autonomously. This fact is exploited by the energy-efficient optimal spectrum balancing algorithm (EEOSB) [15], which solves Problem (8) to optimality.

IV. ROBUST SPECTRUM MANAGEMENT FOR ENERGY MINIMIZATION

We begin our development of energy-efficient robust DSM by introducing uncertainty in the form of a vector $\tilde{\mathbf{G}}_u^c \in \mathcal{R}_+^U$ of *uncertain* crosstalk coefficients to user u on carrier c normalized by the direct channel coefficient, where again $\tilde{G}_{uu}^c = 0$. Based thereupon we extend the nominal problem (2) to its “robust counterpart,” referred to as the primal robust problem (PRP), given as

$$\begin{aligned} & \underset{\mathbf{p}, \mathbf{b}}{\text{minimize}} \quad \sum_{u \in \mathcal{U}} w_u \sum_{c \in \mathcal{C}} p_u^c \\ & \text{subject to} \quad \sum_{c \in \mathcal{C}} b_u^c \geq R_u, \quad \forall u \in \mathcal{U}, \\ & \quad \log_2 \left(1 + \frac{p_u^c}{\Gamma((\mathbf{p}^c)^T \tilde{\mathbf{G}}_u^c + N_u^c)} \right) \geq b_u^c, \\ & \quad \forall u \in \mathcal{U}, \quad c \in \mathcal{C}, \quad \forall \tilde{\mathbf{G}}_u^c \in \mathcal{G}_u^c \\ & \quad \mathbf{0} \preceq \mathbf{p} \preceq \bar{\mathbf{p}}, \\ & \quad b_u^c \in \mathcal{B}_u^c, \quad \forall u \in \mathcal{U}, \quad c \in \mathcal{C} \end{aligned} \quad (10)$$

where $\mathcal{G}_u^c \ni \tilde{\mathbf{G}}_u^c$ denotes the uncertainty set of feasible normalized crosstalk coefficients. Without loss of generality we may restrict ourselves to convex uncertainty sets as stated by the following proposition.

Proposition 1: The worst-case rate $r_u^c(\mathbf{p}^c)$ is invariant when replacing the uncertainty set \mathcal{G}_u^c by its convex hull $\text{conv}(\mathcal{G}_u^c)$.

Proof: First, we note the independence among users in terms of uncertainty sets and target-rate constraints, and that $r_u^c(\mathbf{p}^c)$ is monotonously decreasing in the interference term $(\mathbf{p}^c)^T \tilde{\mathbf{G}}_u^c$. Hence, the worst-case can be constructed by maximizing this interference term. Assuming

$$\tilde{\mathbf{G}}_u^{c,*} = \underset{\tilde{\mathbf{G}}_u^c \in \mathcal{G}_u^c}{\text{argmax}} (\mathbf{p}^c)^T \tilde{\mathbf{G}}_u^c \quad (11)$$

using Carathéodory’s theorem [21, Prop. B.6] and remembering that $\tilde{G}_{uu}^c = 0$, $\forall \tilde{\mathbf{G}}_u^c \in \mathcal{G}_u^c$, we have that

$$\begin{aligned} & \max_{\tilde{\mathbf{G}}_u^c \in \text{conv}(\mathcal{G}_u^c)} \left\{ (\mathbf{p}^c)^T \tilde{\mathbf{G}}_u^c \right\} \\ & = \max_{\alpha_i \geq 0, \sum_i \alpha_i = 1, \tilde{\mathbf{G}}_u^{c,(i)} \in \mathcal{G}_u^c} \left\{ (\mathbf{p}^c)^T \sum_{i=1}^U \alpha_i \tilde{\mathbf{G}}_u^{c,(i)} \right\} \end{aligned} \quad (12)$$

$$= \max_{\alpha_i \geq 0, \sum_i \alpha_i = 1, \tilde{\mathbf{G}}_u^{c,(i)} \in \mathcal{G}_u^c} \left\{ \sum_{i=1}^U \alpha_i (\mathbf{p}^c)^T \tilde{\mathbf{G}}_u^{c,(i)} \right\} \quad (13)$$

$$\leq (\mathbf{p}^c)^T \tilde{\mathbf{G}}_u^{c,*} \quad (14)$$

which concludes the proof. \square

As mentioned, our notation implicitly assumes independence of uncertainty among users and carriers. The projection of the global uncertainty onto uncertainties per user is natural, since the rate constraints have to be fulfilled for each user separately and an uncertainty correlation among users is irrelevant for feasibility under parameter uncertainty. The independence assumption among vectors $\tilde{\mathbf{G}}_u^c$, $\forall c \in \mathcal{C}$, was made to allow an analytic treatment that is independent of the underlying estimation process.

A. Uncertainty Regions

In this paper, we have chosen a *multiplicative* model of uncertainty in the crosstalk coefficients. This choice captures for example arbitrary temporal changes of crosstalk coefficients or an anticipated percental estimation error. A different approach would have been to model uncertainty using an additive error measure. Assuming a norm constraint on the additive errors one obtains a similar convex subproblem formulation as we will get for ellipsoidal uncertainty, as shown in [13] for single-carrier power control. However, to get new insights into the resulting robust problem formulation we base our derivations on a multiplicative formulation. Furthermore, we may also regard this choice as a way to incorporate worst-case changes in the power-allocation of other users, e.g., due to changes of their direct channel coefficients. Finally we note that qualitatively the specific formulation of uncertainty will not alter the main conclusions we draw from this work.

1) *Ellipsoidal Uncertainty Sets*: We will first derive and analyze an uncertainty set in the shape of an ellipsoid. This shape is commonly used due to its relation to Gaussian probability distributions. It was further chosen for its tractability and representativeness for convex uncertainty regions with *interdependence* of worst-case coefficients. Under a multiplicative (percental) uncertainty of normalized crosstalk coefficients relative to their nominal value, the uncertainty set is given by (cf. Fig. 1)

$$\mathcal{G}_u^c = \left\{ \tilde{\mathbf{G}}_u^c \mid \tilde{\mathbf{G}}_u^c = \mathbf{G}_u^c + \text{diag}(\mathbf{G}_u^c) \boldsymbol{\eta}_u^c, \|\boldsymbol{\eta}_u^c\|_2 \leq \varepsilon_u \right\} \quad (15)$$

where $\boldsymbol{\eta}_u^c \in \mathcal{R}^U$, $\text{diag}(\mathbf{G}_u^c)$ denotes the diagonal matrix constructed by the elements of \mathbf{G}_u^c , and $\varepsilon \in \mathcal{R}_+^U$ contains the uncertainty parameters of all users. Note that due to positivity of variables p_u^c it is sufficient to restrict our attention to values $\boldsymbol{\eta}_u^c \succeq \mathbf{0}$. A robust per-carrier power-allocation subproblem in the form of (3) can hence be posed as

$$\begin{aligned} & \underset{\mathbf{p}^c \succeq \mathbf{0}}{\text{minimize}} && \sum_{u \in \mathcal{U}} p_u^c \\ & \text{subject to} && (\mathbf{I} - (\mathbf{F}^c + \Delta \mathbf{F}^{c,\text{ell}})) \mathbf{p}^c \succeq \mathbf{n}^c, \\ & && \forall \boldsymbol{\eta}_u^c \in \{\tilde{\boldsymbol{\eta}}_u^c \in \mathcal{R}_+^U \mid \|\tilde{\boldsymbol{\eta}}_u^c\|_2 \leq \varepsilon_u\}, \\ & && \forall u \in \mathcal{U} \end{aligned} \quad (16)$$

where $\Delta \mathbf{F}^{c,\text{ell}} \in \mathcal{R}^{U \times U}$, $\forall c \in \mathcal{C}$, and

$$\Delta F_{uv}^{c,\text{ell}} = \Gamma \gamma_u^c \tilde{\eta}_{uv}^c G_{uv}^c. \quad (17)$$

In this specific case, the semi-infinite problem (16) can be cast in a minimax form [22]. Conferring to PRP in (10), the model parameters maximizing the interference can be analytically derived using the following relations:

$$\begin{aligned} & \max_{\tilde{\mathbf{G}}_u^c \in \mathcal{G}_u^c} (\mathbf{p}^c)^T \tilde{\mathbf{G}}_u^c \\ & = (\mathbf{p}^c)^T \mathbf{G}_u^c + \max_{\{\tilde{\boldsymbol{\eta}}_u^c \mid \|\tilde{\boldsymbol{\eta}}_u^c\|_2 \leq \varepsilon_u\}} (\mathbf{p}^c)^T \text{diag}(\mathbf{G}_u^c) \tilde{\boldsymbol{\eta}}_u^c \\ & = (\mathbf{p}^c)^T \mathbf{G}_u^c + \varepsilon_u \|\text{diag}(\mathbf{G}_u^c) \mathbf{p}^c\|_2. \end{aligned} \quad (18)$$

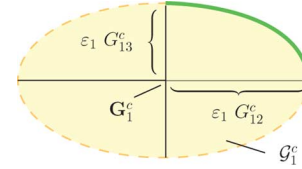


Fig. 1. Schematic of an ellipsoidal uncertainty region \mathcal{G}_u^c for $u = 1$ and $U = 3$, where the possible interference-maximizing set lying on the relative boundary of \mathcal{G}_u^c is emphasized.

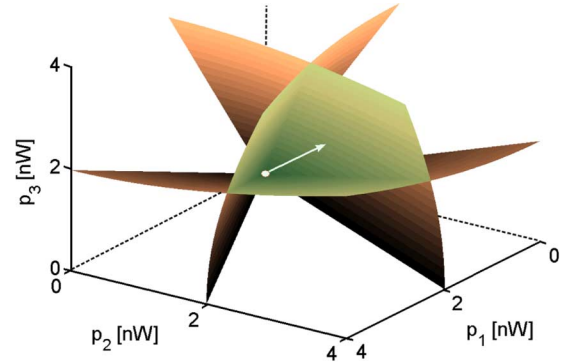


Fig. 2. Illustration of the boundaries of rate-constraint SOCs and the feasible power region (lightly shaded) for robust single-carrier power allocation with ellipsoid-shaped uncertainty of crosstalk coefficients.

Hence, the constraint set in (16) can be written more compactly as the product set of second-order cone (SOC) [23] constraints, and Problem (16) can be rewritten as

$$\begin{aligned} & \underset{\mathbf{p}^c \succeq \mathbf{0}}{\text{minimize}} && \sum_{u \in \mathcal{U}} p_u^c \\ & \text{subject to} && p_u^c - \Gamma \gamma_u^c (\mathbf{p}^c)^T \mathbf{G}_u^c \\ & && \quad - \varepsilon_u \Gamma \gamma_u^c \|\text{diag}(\mathbf{G}_u^c) \mathbf{p}^c\|_2 \geq n_u^c, \\ & && \forall u \in \mathcal{U}. \end{aligned} \quad (19)$$

Note that in order to solve the resulting SOC-program using standard cone-solvers such as MOSEK [24], one needs to further reformulate the problem by introducing extra variable-vectors for each term $\text{diag}(\mathbf{G}_u^c) \mathbf{p}^c$, $\forall u \in \mathcal{U}$. Fig. 2 schematically illustrates a symmetric robust power-allocation problem on carrier $c = 1$ for $U = 3$ users each located at 300 m distance from the deployment point, $\varepsilon_u = 300$, $b_c^u = 1$, $\forall u \in \mathcal{U}$, and all other simulation parameters as specified in Section V. Note that the high uncertainty-radius was chosen to emphasize the shape of the constraint set. The lightly shaded area is the intersection of 3-SOCs as defined by the users' constraints in Problem (19), the arrow represents the constant gradient of the cost to be minimized and the marked point indicates the unique optimum.

2) *Box-Shaped Uncertainty Sets*: The second type of uncertainty regions we will use are box-shaped ones, given by

$$\mathcal{G}_u^c = \left\{ \tilde{\mathbf{G}}_u^c \mid \tilde{\mathbf{G}}_u^c = \mathbf{G}_u^c + \text{diag}(\mathbf{G}_u^c) \tilde{\boldsymbol{\eta}}_u^c, \tilde{\eta}_{uv}^c \leq \varepsilon_u, \forall v \in \mathcal{U} \right\} \quad (20)$$

where $\tilde{\boldsymbol{\eta}}_u^c \in \mathcal{R}^U$. Note that we use the same uncertainty parameters $\varepsilon \in \mathcal{R}_+^U$ as in the previous section, to arrive at a fair comparison to ellipsoidal uncertainty sets and extract the effect of their

different shapes. This can be interpreted as column-wise uncertainty, where column refers to the constraint matrix in linear constraints. Furthermore, this most pessimistic uncertainty set is equivalent to multiplying the crosstalk coefficients \mathbf{G}_u^c by $(1 + \varepsilon_u)$, $\forall c \in \mathcal{C}$, $u \in \mathcal{U}$, and can be considered as a margin on the crosstalk noise. The corresponding robust power-allocation problem can then be posed in a straightforward manner as

$$\begin{aligned} & \underset{\mathbf{p}^c \succeq \mathbf{0}}{\text{minimize}} && \sum_{u \in \mathcal{U}} p_u^c \\ & \text{subject to} && p_u^c - (1 + \varepsilon_u) \Gamma \gamma_u^c (\mathbf{p}^c)^T \mathbf{G}_u^c \geq n_u^c, \\ & && \forall u \in \mathcal{U} \end{aligned} \quad (21)$$

which notably has the advantage of remaining a linear program. Comparing the robust subproblems in (19) and (21), we see that they differ in a single term in the constraint functions. From triangle inequality, convexity of the square-function and using $G_{uu}^c = 0$ it holds that

$$\frac{1}{\sqrt{U-1}} (\mathbf{p}^c)^T \mathbf{G}_u^c \leq \|\text{diag}(\mathbf{G}_u^c) \mathbf{p}^c\|_2 \leq (\mathbf{p}^c)^T \mathbf{G}_u^c. \quad (22)$$

Hence, we conclude that the constraint set in (19) is never more restrictive than the constraint set in (21). Therefore, robust power allocation with box-shaped uncertainty can never yield a lower minimum sum-power than one with ellipsoidal uncertainty region when equal uncertainty parameters are used, which also follows directly by inspection of their respective uncertainty sets.

In [9], a cardinality constrained uncertainty concept was proposed. Therein one assumes box-constraints for each coefficient and restricts the number of coefficients which are allowed to deviate from the nominal value. This approach can be used to model the amount of interference in communication systems where users are entering and leaving the system [13]. Hence, if statistics on the number of users active at any time are available, this approach may be used to ensure robustness in DSL systems when additional lines become active. Note, however, that the users becoming active then have to adhere to the spectral allocation foreseen/optimized by the DSM algorithm. When assuming the maximum of $U - 1$ disturbers, however, one falls back to the box-constrained uncertainty model.

B. Implicit Outage Probability Bounds

We can also cast the power-allocation optimization problem (19) for ellipsoidal uncertainty regions in a probabilistic framework [10, Sec. 4.4.2] if we assume independent Gaussian random vectors $\hat{\mathbf{G}}_u^c$, $\forall u \in \mathcal{U}$, $\forall c \in \mathcal{C}$. A probabilistic problem formulation is obtained by replacing ε_u by $\phi^{-1}(1 - \sigma_u)$ and $\text{diag}(\mathbf{G}_u^c)$ by $(\Sigma_u^c)^{(1/2)}$ in (19), where σ_u is the desired outage probability, Σ_u^c being the covariance matrix for coefficients $\hat{\mathbf{G}}_u^c$, and $\phi(\cdot)$ denotes the Gaussian cumulative distribution function with zero mean and unit variance.

We are further interested in an outage probability of a robust solution to (19) with ellipsoidal uncertainty region when the real uncertainty set is box-shaped (cf. (21)), which is *independent* of the exact solutions to (19) and (21). The following

proposition gives loose outage probability bounds under certain assumptions.

Proposition 2: Assume having coefficients

$$\hat{G}_{uv}^c \in [G_{uv}^c(1 - \varepsilon_u), G_{uv}^c(1 + \varepsilon_u)], \quad u, v \in \mathcal{U}, \quad (23)$$

all being independent and symmetrically distributed in the interval. The outage probabilities $\sigma_u = \sigma$, $\forall u \in \mathcal{U}$, according to a robust solution of Problem (19) are bounded by

$$\sigma \leq \frac{1}{\sqrt{e}}, \quad (24)$$

independently of scenario, uncertainty parameters ε_u and solution $\mathbf{p}^{c,*}$, where e is Euler's number. Another bound of the outage probability is obtained by restriction to the case of independent and uniformly distributed coefficients \hat{G}_{uv}^c as

$$\sigma = 1 - \frac{V^{\text{ball}}(U-1)}{V^{\text{box}}(U-1)} \quad (25)$$

where $V^{\text{ball}}(d)$ and $V^{\text{box}}(d)$ are the volumes of the unit ball and the unit box in d dimensions.

See Appendix A for a proof.

We note that the bound in (25) for uniform distributions is monotonously increasing in U . Eventually it becomes looser than the more general bound in (24) when $U \geq 4$.

C. Feasibility Conditions

Using the effect of uncertainty on the power-allocation constraint in (21) together with the uncertainty region in (20) and the feasibility criterion (7) for the nominal power-allocation problem in (3) it is straightforward to derive the following sufficient feasibility conditions for the robust case with multiplicative uncertainty.

Proposition 3: A robust, single-carrier power-allocation is feasible in ellipsoidal uncertainty constrained Problem (19) and in box-uncertainty constrained Problem (21) with uncertainty parameters $\boldsymbol{\varepsilon} \in \mathcal{R}_+^U$ if

$$\|\mathbf{F}^c\|_2 < \frac{1}{1 + \sqrt{U} \|\boldsymbol{\varepsilon}\|_2}. \quad (26)$$

Furthermore, if $\varepsilon_u = \varepsilon$, $\forall u \in \mathcal{U}$, then a sufficient condition for ellipsoidal uncertainty is given by

$$\rho(\mathbf{F}^c) < \frac{1}{1 + \varepsilon}. \quad (27)$$

For box-shaped uncertainty sets (27) is sufficient and additionally necessary.

See Appendix B for a proof.

We note that the first condition is different to the convergence result in [13] where additive instead of multiplicative uncertainty was assumed, while the latter one is equal to [25, Lemma 1] on the problem of power control with SINR margins.

D. Sensitivity Analysis of the Dual Function

In this section we will perform a sensitivity analysis for the dual objective in (8) and derive a subgradient w.r.t. the robustness parameters ε_u , $u \in \mathcal{U}$. Sensitivity analysis is a standard

tool to calculate the local change of the objective to a perturbation of problem-parameters, cf. [10, Ch. 5.6]. Our analysis does however not apply to the primal objective due to the in general nonzero duality gap of (PRP) in (10). A nonzero duality gap does not necessarily imply the primal suboptimality of primal solutions found by dual optimization. Furthermore, depending on the target-rate assignment the gap may be assumed to be fairly small [15], which motivates the following derivation and also implies the near-optimality of EEOSB.

While we will restrict ourselves now to ellipsoidal uncertainty regions, sensitivity results for box-shaped uncertainty sets can be obtained in a similar way. We consider the partial dual of problem PRP in (10), which is similar to the nominal dual problem (8), but further separates the minimization over \mathbf{p} and relaxes the robust, per-carrier SINR-constraints. Regarding Problem (19), this dual robust problem (DRP), for which we will present a solution algorithm in Section IV-E, can be written as

$$\underset{\boldsymbol{\lambda} \geq \mathbf{0}}{\text{maximize}} \quad \underset{b_u^c \in \mathcal{B}_u^c, \forall c \in \mathcal{C}, u \in \mathcal{U}}{\text{minimize}} \quad \sum_{c \in \mathcal{C}} q_{\text{rob}}^c(\boldsymbol{\lambda}, \mathbf{b}^c) \quad (28)$$

where

$$q_{\text{rob}}^c(\boldsymbol{\lambda}, \mathbf{b}^c) = \underset{\boldsymbol{\mu}^c \geq \mathbf{0}}{\text{maximize}} \quad \underset{\mathbf{p}^c \geq \mathbf{0}}{\text{minimize}} \quad L_{\text{rob}}^c(\mathbf{p}^c, \mathbf{b}^c, \boldsymbol{\lambda}, \boldsymbol{\mu}^c) \quad (29)$$

and where $\boldsymbol{\mu}^c \in \mathcal{R}^U$, $c \in \mathcal{C}$, is the vector of per-carrier power-allocation constraint multipliers. Furthermore, L_{rob}^c is given by

$$\begin{aligned} L_{\text{rob}}^c(\mathbf{p}^c, \mathbf{b}^c, \boldsymbol{\lambda}, \boldsymbol{\mu}^c) &= \sum_{u \in \mathcal{U}} \left(w_u p_u^c + \lambda_u \left(\frac{R_u}{C} - b_u^c \right) \right) \\ &+ \sum_{u \in \mathcal{U}} \mu_u^c \left(\varepsilon_u \Gamma \gamma_u^c \|\text{diag}(\mathbf{G}_u^c) \mathbf{p}^c\|_2 \right. \\ &\quad \left. - p_u^c + \Gamma \gamma_u^c (\mathbf{p}^c)^T \mathbf{G}_u^c + n_u^c \right). \quad (30) \end{aligned}$$

The following proposition defines a subgradient for the dual objective in (28) w.r.t. the uncertainty parameters $\boldsymbol{\varepsilon}$.

Proposition 4: Let \mathbf{p}^* , \mathbf{b}^* , $\boldsymbol{\lambda}^*$ and $\boldsymbol{\mu}^{c,*}$ be optimal variables for the dual robust DSM problem (28) and the per-carrier dual subproblems (29), respectively. Then, a subgradient $\mathbf{g} \in \mathcal{R}^U$ of the optimal dual cost $\sum_{c \in \mathcal{C}} q_{\text{rob}}^c(\boldsymbol{\lambda}^*, \mathbf{b}^{c,*})$ w.r.t. $\boldsymbol{\varepsilon}$ is given by

$$g_u = \sum_{c \in \mathcal{C}} \mu_u^{c,*} \Gamma (2^{b_u^{c,*}} - 1) \|\text{diag}(\mathbf{G}_u^c) \mathbf{p}^{c,*}\|_2, \quad \forall u \in \mathcal{U}. \quad (31)$$

See Appendix C for a proof.

The sensitivity information in (31) can be readily used after optimization of (28) (e.g., by our robust DSM algorithm presented in Section IV-E) to predict changes in the optimal dual objective for small perturbations of $\boldsymbol{\varepsilon}$, cf. Section V-B for a visualization. Notably, as we see in (31), the subgradient information demands the knowledge of optimal dual multipliers $\boldsymbol{\mu}^c, \forall c \in \mathcal{C}$, at the bit-allocation optimized by DSM.

An idea to further exploit this subgradient information is in a scheme where uncertainty parameters and energy are optimized jointly. Similarly as in [25], an ε -adaptation stage on top of Problem (28) would target the minimization of a weighted

sum of sum-power and a user-dependent convex and monotonously decreasing function of robustness (parameters ε). Since the choice of such for energy optimization in DSL systems is out of the scope of this work, we only refer to similar multiobjective decomposition schemes developed in [26] and [27].

E. Robust EEOSB Algorithm Description

We will now describe the robust DSM algorithm used to solve (28). It consists of two hierarchical problems as seen in (28) and (29), where the top-level algorithm used to solve (28) is similar to EEOSB [15] and summarized in Algorithms 1 and 2. The low-level problem is the convex power-allocation problem in (19) (or (21), respectively) and solved by standard solvers, cf. Section IV-A. The EEOSB algorithm in Algorithm 1 is based on the (dual) optimal spectrum balancing (OSB) algorithm in [16], adapted for our problem (2). Algorithm 2 summarizes the exhaustive search subroutine replacing the corresponding subroutine in the original EEOSB algorithm in [15]. More specifically, it is Line 5 which makes the DSM algorithm worst-case robust against uncertainties as specified in Section IV-A by solving (29). In Lines 6 to 8, we check the solution $\tilde{\mathbf{p}}^{c,*}$ obtained from (19) (or (21), respectively) for feasibility and conformity with the spectral mask constraint, compute the per-carrier Lagrangian, and store the best allocations found. Lines 11 to 17 and Lines 18 to 24 simply ensure an exhaustive search of all feasible bit-allocations w.r.t. power and bit-cap constraints, respectively. Note that the feasible bit and power-allocations on all carriers may be precomputed to improve the running time of EEOSB.

Algorithm 1: Robust EEOSB Scheme

```

Initialize:  $\lambda^{\text{Res}}, \lambda^0, \boldsymbol{\lambda}$ 
 $[\boldsymbol{\lambda}, \mathbf{p}, \mathbf{b}] = \mathbf{Bisection}(\boldsymbol{\lambda}, U)$ 


---


Function  $[\boldsymbol{\lambda}, \mathbf{p}, \mathbf{b}] = \mathbf{Bisection}(\boldsymbol{\lambda}, u)$ 
Initialize  $\lambda^{\text{min}} = 0$ 
5:  $[\lambda^{\text{max}}] = \mathbf{SearchMaxMultiplier}(\boldsymbol{\lambda}, u)$ 
   repeat
      $\lambda_u = (\lambda^{\text{max}} - \lambda^{\text{min}}/2)$ 
     if  $u \neq 1$  then  $\{[\boldsymbol{\lambda}, \mathbf{p}, \mathbf{b}] = \mathbf{Bisection}(\boldsymbol{\lambda}, u - 1)\}$ 
     else  $\{[\mathbf{p}, \mathbf{b}] = \mathbf{OptRobustAllocation}(\boldsymbol{\lambda})\}$ 
10:   end if
     if  $\sum_{c \in \mathcal{C}} b_u^c \geq R_u$  then  $\{\lambda^{\text{max}} = \lambda_u\}$ 
     else  $\{\lambda^{\text{min}} = \lambda_u\}$ 
     end if
   until  $((\lambda^{\text{max}} - \lambda^{\text{min}}/\lambda_u) < \lambda^{\text{Res}})$  and  $(\sum_{c \in \mathcal{C}} b_u^c \geq R_u)$ 


---


15: Function  $[\lambda^{\text{max}}] = \mathbf{SearchMaxMultiplier}(\boldsymbol{\lambda}, u)$ 
   Initialize  $\lambda^{\text{max}} = (\lambda^0/2)$ 
   repeat
      $\lambda^{\text{max}} = 2\lambda^{\text{max}}, \lambda_u = \lambda^{\text{max}}$ 
     if  $u \neq 1$  then  $\{[\boldsymbol{\lambda}, \mathbf{p}, \mathbf{b}] = \mathbf{Bisection}(\boldsymbol{\lambda}, u - 1)\}$ 
20:   else  $\{[\mathbf{p}, \mathbf{b}] = \mathbf{OptRobustAllocation}(\boldsymbol{\lambda})\}$ 
     end if
   until  $\sum_{c \in \mathcal{C}} b_u^c \geq R_u$ 


---



```

Algorithm 2: Subroutine for Robust EEOSB

Function[\mathbf{p}, \mathbf{b}] = *OptRobustAllocation*(λ)
for $c = 1$ to C
 Initialize $\hat{\mathbf{b}}^c = \mathbf{0}$, $\text{bEnd} = \text{false}$
while $\text{bEnd} == \text{false}$ **do**
 5: Calculate $\hat{\mathbf{p}}^{c,*}$ by (19) (or (21), respectively)
if (solution $\hat{\mathbf{p}}^{c,*}$ was found) and ($\mathbf{p}^{c,*} \preceq \bar{\mathbf{p}}$) **then**
 Calculate $L^c(\hat{\mathbf{p}}^{c,*}, \hat{\mathbf{b}}^c, \lambda)$ as in (9)
 $\{\mathbf{p}^c, \mathbf{b}^c\} = \underset{\{\check{\mathbf{p}}^c, \check{\mathbf{b}}^c\} \in \{\{\hat{\mathbf{p}}^{c,*}, \hat{\mathbf{b}}^c\}, \{\mathbf{p}^c, \mathbf{b}^c\}\}}{\text{argmin}} \{L^c(\check{\mathbf{p}}^c, \check{\mathbf{b}}^c, \lambda)\}$
 $\hat{b}_1^c = \hat{b}_1^c + 1$
 10: **else**
 $u = 1$
while $\hat{b}_u^c == 0$ **do** $\{u = u + 1\}$
end while
if $u < U$ **then** $\{\hat{b}_u^c = 0, \hat{b}_{u+1}^c = \hat{b}_{u+1}^c + 1\}$
 15: **else** $\{\text{bEnd} = \text{true}\}$
end if
end if
for $u = 1$ to $U - 1$ **do**
if $\hat{b}_u^c > \bar{b}_u^c$ **then** $\{\hat{b}_u^c = 0, \hat{b}_{u+1}^c = \hat{b}_{u+1}^c + 1\}$
 20: **end if**
if $\hat{b}_U^c > \bar{b}_U^c$ **then** $\{\text{bEnd} = \text{true}\}$
end if
end for
end while
 25: **end for**

The following proposition justifies the sufficiency of checking the solutions to Problems (19) (or (21), respectively) against the spectral mask constraints (cf. Line 6 in Algorithm 2) in order to conclude the nonexistence of any feasible allocation below the mask constraints.

Proposition 5: Assume the optimal solution $\mathbf{p}^{c,*}$ to a power-allocation subproblem (19) (or (21), respectively) and additional spectral mask constraints $\bar{\mathbf{p}}^c$ on carrier c . Then

$$\exists u \in \mathcal{U} : p_u^{c,*} > \bar{p}_u^c \iff \nexists \mathbf{p}^c \in \mathcal{P}^c : \mathbf{p}^c \preceq \bar{\mathbf{p}}^c \quad (32)$$

where \mathcal{P}^c denotes the feasible set in (19) (or (21), respectively). Furthermore, it holds that $\hat{\mathbf{p}}^{c,*} \preceq \check{\mathbf{p}}^{c,*} \preceq \bar{\mathbf{p}}^{c,*}$, where $\hat{\mathbf{p}}^{c,*}$, $\check{\mathbf{p}}^{c,*}$ and $\bar{\mathbf{p}}^{c,*}$ are the solutions to nominal problem (3) and robust problems (19) and (21), respectively.

See Appendix D for a proof.

Proposition 5 implies the Pareto optimality of a solution to Problem (3) as a special case, a result also proven in [28, Prop. 1].

F. Complexity and Distributiveness

Complexity is one practical point to be considered for the application of both our uncertainty regions to EEOSB [15]. For the naive implementation using exhaustive search of any bit-allocation feasible w.r.t. the bit-cap constraints, we have a com-

plexity $O(\sum_{c \in \mathcal{C}} \prod_{u \in \mathcal{U}} \bar{b}_u^c)$ per dual iteration in Algorithm 1. Differently, the search for feasible bit-allocations in Algorithm 2 may have a lower complexity as infeasibility w.r.t. spectral mask constraints, evaluated in Line 6, indicates also the infeasibility of several higher bit-allocations, cf. Lines 11 to 17. Proposition 5 has shown that the powers under robust power-allocation are *element-wise* higher than or equal to the nominal ones in (6). This explains why robust EEOSB typically needs to search less bit-allocations and is therefore faster than the original EEOSB algorithm if the power-allocations for all feasible bit-allocations are precomputed. For the same reasons also the two considered uncertainty approaches may differ in their search complexity.

For each evaluated bit-allocation we face the subproblem of computing a robust power-allocation in Line 5 of Algorithm 2. The latter has in the case of a SOC-problem [23] as well as in case of a matrix inversion an asymptotic complexity of $O(U^3)$, assuming the matrix inversion for the case of box-uncertainty is performed by Gaussian elimination. The practical running time to solve the respective subproblems however is to our experience several magnitudes higher in case of ellipsoidal uncertainty.

As the EEOSB algorithm is only practical for a very moderate number of users, it is also interesting to see how the two approaches are implementable in schemes with lower complexity. When applying an iterative scheme over users as done in energy-efficient iterative spectrum balancing (EEISB) [15], we recognize that both approaches suddenly have a similar complexity for evaluating the robust power-allocation for a certain bit-allocation. In case of ellipsoidal uncertainty regions we do not need to solve the SOC-problem (19) anymore, but instead evaluate the feasible power-allocation for user u , $\forall c \in \mathcal{C}$, $b_u^c \in \mathcal{B}_u^c$, by

$$p_u^c = \Gamma \gamma_u^c (\mathbf{p}^c)^T \mathbf{G}_u^c + \varepsilon_u \Gamma \gamma_u^c \|\text{diag}(\mathbf{G}_u^c) \mathbf{p}^c\|_2 + n_u^c \quad (33)$$

where notably the right-hand side does not depend on p_u^c , cf. Problem (19).

Besides computational complexity, another practical point is the possibility of distributed implementations. The continuous and heuristic energy-efficient spectrum balancing (EESB) algorithm in [3] theoretically allows for a semi-distributed implementation based on modems measuring their total noise and a spectrum management center (SMC) having information about cross-channel couplings. This message-exchange scheme naturally carries over to box-constrained uncertainty, where each modem u additionally has to measure the background noise separately to derive the pure crosstalk noise and the virtual noise term $\Gamma((1 + \varepsilon_u)(\mathbf{p}^c)^T \mathbf{G}_u^c + N_u^c)$, cf. (21), and appropriately scales the feedback messages to the SMC. Similarly an iterative water-filling type of algorithm [15] can be deployed under box-shaped uncertainty. Unfortunately there is no way to efficiently derive or measure the term $\|\text{diag}(\mathbf{G}_u^c) \mathbf{p}^c\|_2$ distributively, which is why both distributed schemes EESB and iterative water-filling lose their attractiveness under the ellipsoidal uncertainty approach (or in fact *any* other non-box-shaped uncertainty region).

Hence, we see that the SOC-constraints in (19) couple the power-allocations of all users on each carrier. The distributed robust power-control algorithm for additive, ellipsoid-shaped uncertainty in [13] allows for delayed messaging of the coupling

terms. Still, in a multicarrier system this means that a user has to transmit the whole optimized power-allocation \mathbf{p}_u after his iteration in order for other users being able to make their decisions distributively. Despite the negative results in terms of distributiveness for ellipsoidal uncertainty sets, in Section V we will still consider these sets in order to compare different levels of uncertainty. We omitted any discussion of convergence for the mentioned robust iterative schemes beyond the simulation results in Section V. This is because convergence conditions usable in practice are even not available for the nominal iterative algorithms.

V. SIMULATIONS

The aim of the following simulations is to evaluate and compare the proposed robust DSM approaches (optimization problem DRP in (28) with box-shaped or ellipsoidal uncertainty sets) in terms of the extra energy consumed or max-min rate lost. We consider two VDSL upstream scenarios, where three users are located at 200, 400, and 600 m, and ten users located at 100, 200, ..., 1000 m distance from the deployment point, respectively. We note that there is no difference between ellipsoidal and box-shaped uncertainty regions when only two users are considered. However, the consideration of a three-user scenario already allows to study the differences between the considered uncertainty regions by the near-optimal robust EEOSB algorithm in Algorithm 1 using the robust power-allocation subroutine in Algorithm 2, while keeping the combinatorial complexity at a manageable level. The ten-user scenario will be simulated using the EEISB algorithm [15] and the simple modification of the considered crosstalk as given in (33) for ellipsoidal uncertainty sets, or simply scaled crosstalk coefficients for box-shaped uncertainty sets, respectively. The simulation parameters were chosen according to the ETSI VDSL standard [29], with an SNR-gap $\Gamma = 12.8$ dB and two transmission bands as defined in band plan 997. The background noise comprised ETSI VDSL noise A added to a constant noise floor at -140 dBm/Hz. For ease of exposition, we have used an identical uncertainty parameter for all users, i.e., $\varepsilon_u = \varepsilon, \forall u \in \mathcal{U}$. The values for the uncertainty parameters ε will be varied around the value one, based on real world crosstalk parameter uncertainties indicated in [30].

A. Robust Power Allocation

Fig. 3 illustrates the optimal PSDs for an uncertainty-parameter $\varepsilon = 4$ (which under box-shaped uncertainty sets is equivalent to a crosstalk noise level virtually increased by approximately 7 dB) and target-rate $R_u = 7.5$ kb/DMT-symbol (or, equivalently, 30 Mb/s) for all three users. As intuitively expected, the bit-allocation over carriers tends to avoid crosstalk when a robust power allocation is used. Hence, large parts of the spectrum are then divided among the users. Furthermore, the spectral mask constraint prohibits the loading of more bits in the upper subband and hence also parts of the lower subband with less attenuation and partly lower crosstalk coefficients are used exclusively by a single user.

B. Energy Cost for Robustness

The extra robustness will certainly have a price in terms of a higher power consumption. In Fig. 4 we exemplify this “price

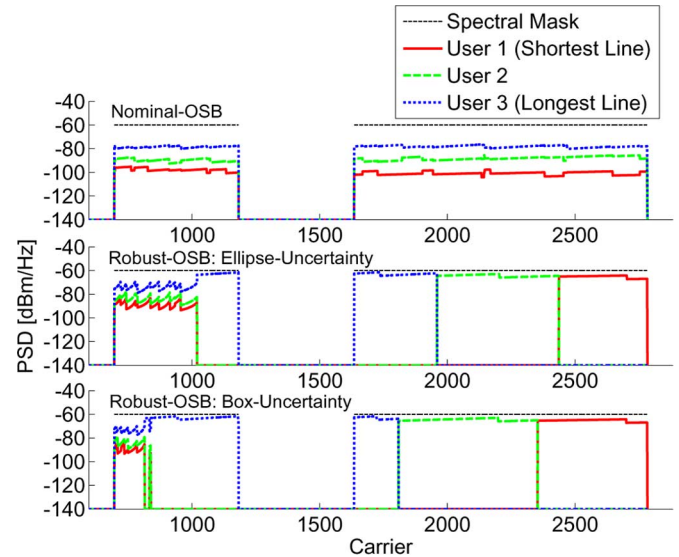


Fig. 3. Comparison of optimal power-allocations over carriers for an uncertainty parameter $\varepsilon = 4$ and a target-rate of 30 Mb/s for all three users.

of robustness” in DSM under ellipsoid/box-shaped uncertainty regions for equal target rates. Considering Fig. 4(a) obtained by the near-optimal robust EEOSB algorithm, we see that the increase in sum-power from the nominal solution under uncertainty is negligible at lower target rates. This is due to the fact that crosstalk noise levels can be kept low as well at an optimum power-allocation. The same holds for small uncertainty radii under both considered uncertainty-region shapes over the whole rate range. As discussed in Section IV box-shaped uncertainty regions yield a higher level of conservatism compared to ellipsoidal ones, but also demand an extra energy consumption for the additional worst-case robustness. The difference between the uncertainty set shapes in terms of sum-power is most notable for medium-size uncertainty parameters (e.g., $\varepsilon = 1$, corresponding to 100% uncertainty in the crosstalk coefficients or ≈ 3 dB crosstalk noise margin under box-shaped uncertainty sets). For low/high values of parameter ε the differences vanish as either the impact on the solution to the robust per-carrier power-allocation problems is small (the number of loaded bits per carrier is low), or spectrum management allows to separate users over carriers where they would heavily interfere. Note, however, that the difference between the uncertainty shapes at medium uncertainties also vanishes at higher target rates if we only sufficiently relax the spectral mask constraints.

In Fig. 4(b), we see that under the suboptimal EEISB algorithm the difference between the uncertainty shapes does not vanish for the shown medium/high uncertainty values, also not if one neglects the spectral mask constraint. This can be explained by both, its suboptimality and the correspondingly smaller rate region.

Fig. 5 compares both uncertainty sets by showing the dependency on parameter ε , again using our robust EEOSB algorithm. This plot corresponds to a vertical cut through the curves in Fig. 4(a) at a rate of 30 Mb/s, where for $\varepsilon = 1$ we have added the subgradient information computed by (31). Notably the fixed target rate is relatively large for the chosen scenario, emphasizing again the lower energy consumption of ellipsoidal uncertainty sets in the medium uncertainty range. The extra power

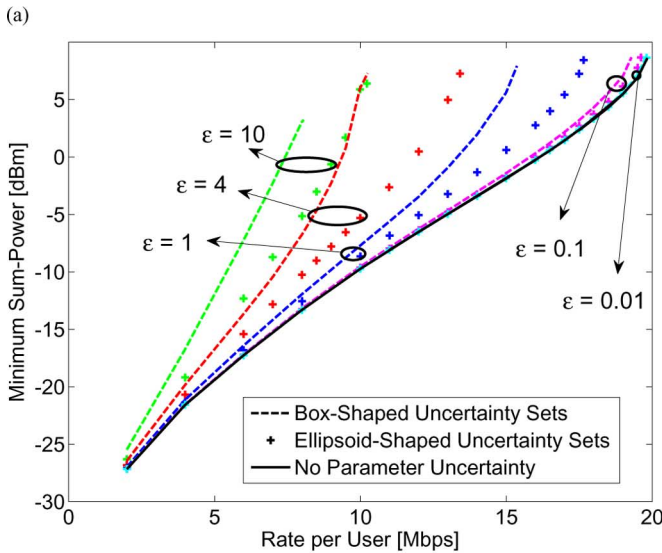
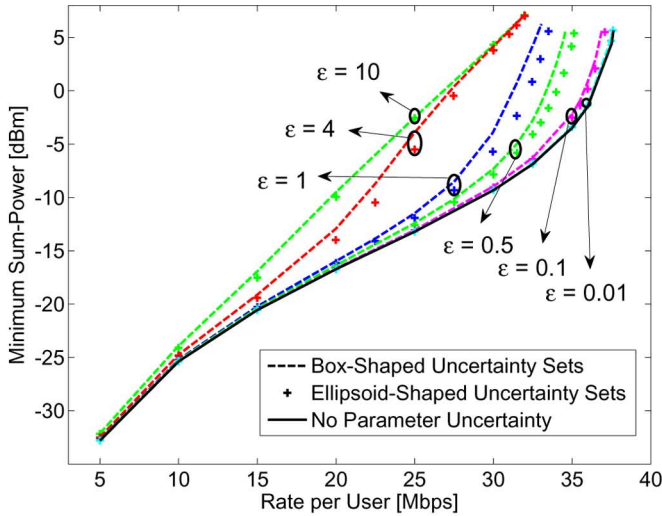


Fig. 4. Minimum sum-power of robust optimization for box/ellipsoid-shaped uncertainty sets with equal target-rates: (a) in the three-user VDSL scenario and (b) in the ten-user VDSL scenario.

investment for robustness compared to the nominal sum-power can be seen to be ≤ 2 dB under both uncertainty sets for values of the uncertainty parameter $\varepsilon \leq 0.5$. The largest difference between the two set shapes among the simulated uncertainty values ($\approx 610 \mu\text{W}$) can be seen for a medium-size uncertainty $\varepsilon = 2$. At the highest shown uncertainty $\varepsilon = 10$ the bit allocation is orthogonal among users and higher uncertainties would hence not further increase the necessary sum-power.

C. Worst-Case Rate Loss

In this section, we will investigate the relationship between the maximal worst-case rate loss over users w.r.t. the target-rates R_u , $u \in \mathcal{U}$, and the necessary energy investment for robustness. For this purpose, we will compute nominal solutions to nominal problem (8) and regard the rate loss when applying worst-case crosstalk parameters. When calculating this rate loss, we distinguish between worst-case crosstalk noise under ellipsoidal and box-shaped uncertainty regions with identical uncertainty parameter ε , respectively, as indicated by “Ellipse” and “Box”

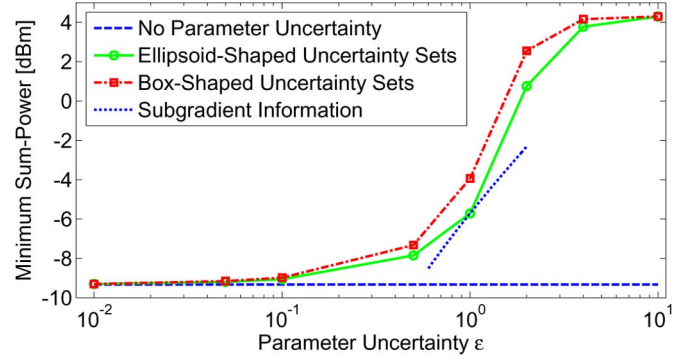


Fig. 5. Dependency of minimum sum-power on uncertainty parameter ε in a three-user VDSL scenario for equal target-rates of 30 Mb/s; subgradient information at $\varepsilon = 1$ was computed using (31).

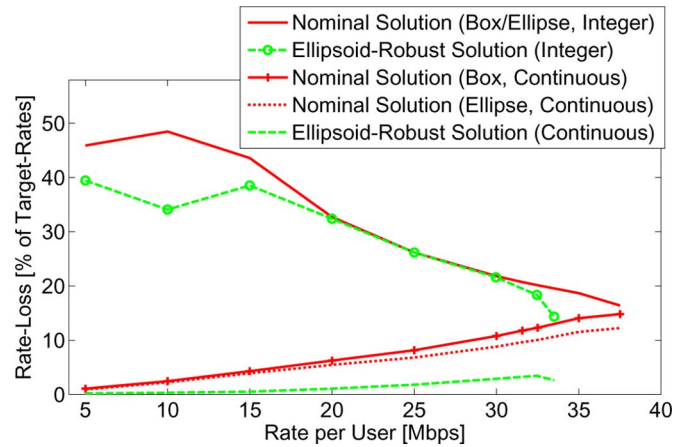


Fig. 6. Maximal rate loss per user under worst-case crosstalk parameters compared to target rates ($\varepsilon = 1$, box/ellipsoid-shaped uncertainty set, continuous/integer worst-case bit allocation).

in Fig. 6, cf. also Problems (19) and (21). For the robust solution under ellipsoidal uncertainty regions, we can also compute a worst-case rate loss, namely by picking worst-case parameters from a box-shaped uncertainty region with corresponding uncertainty parameter ε . Another subtlety is whether the bits per carrier after considering worst-case parameters are rounded to the nearest lower integer or not, indicated by the terms “Integer” and “Continuous” in Fig. 6, respectively.

It can be noticed that the worst-case rate loss of the nominal solution under integer rounding of the worst-case bit allocation is quite dramatic, cf. Fig. 6. It is naturally decreasing in the percent of the target rates as the number of loaded bits increases and the impact of the rounding procedure decreases. We find the rate loss of the robust solution for ellipsoidal uncertainty regions comparably high when worst-case parameters from box-shaped regions are assumed and the mentioned rounding procedure applied afterwards.

We will now consider only the minimum rates of nominal/robust solutions under box-shaped uncertainty sets and without the following rounding of the bit allocation. As an example, selecting $R_u = 30$ Mb/s in the three-user scenario, we see that robust EEOSB with ellipsoidal uncertainty regions prevents more than 70% of the worst-case rate loss the nominal solution would suffer, while saving around 50% of the extra energy for robust EEOSB under box-shaped uncertainty regions, cf. Table I and Figs. 4(a) and 6. Similarly, regarding the ten-user scenario and

TABLE I

COMPARISON OF MINIMUM (WORST-CASE) RATES PER USER AND SUM-POWER FOR $\varepsilon = 1$ IN A SCENARIO WITH (A) THREE USERS AND $R_u = 30$ Mb/s, OR (B) TEN USERS AND $R_u = 12$ Mb/s, $\forall u \in \mathcal{U}$; NOMINAL AND ROBUST SOLUTIONS UNDER BOX-SHAPED/ELLIPTOIDAL UNCERTAINTY REGIONS; WORST-CASE CROSSTALK PARAMETERS TAKEN FROM BOX-SHAPED UNCERTAINTY REGIONS

Scenario	Worst-Case Rate [Mbps]		Sum-Power [dBm] ([mW])	
	(A)	(B)	(A)	(B)
Box	30	12	-3.93 (0.40)	-3.46 (0.45)
Ellipsoid	29.14	10.96	-5.71 (0.27)	-5.05 (0.31)
Nominal	26.77	10.04	-9.32 (0.12)	-6.53 (0.22)

$R_u = 12$ Mb/s, we find that robust EEOSB with ellipsoidal uncertainty regions prevents more than 50% of the worst-case rate loss while saving around 60% of the extra energy, cf. Table I and also Fig. 4(b).

D. Comparison Between Robust DSM and Heuristic Search

Another question one may ask is how much we save by considering uncertainty in crosstalk coefficients directly compared to other strategies which also increase robustness. A simple heuristic we may think of for achieving feasibility under parameter uncertainty is to search for (uniformly for all users) *increased* target rates to the nominal problem (8) until we find a nominal solution that achieves the *original* target rates under worst-case crosstalk parameters. Furthermore, we would like these increased target rates to be as low as possible to save energy. Hence, we performed a search on target rates with adaptive step-size and in each iteration solve the dual *nominal* problem (8) using the standard EEOSB algorithm. The target-rate search halts if the (absolute, averaged over users) search uncertainty in *worst-case* rates relative to the original target rate falls below 10^{-5} . By worst-case rates we understand, similarly as in the previous section, the achieved rate under worst-case parameters for the nominal solution under increased target rates and following rounding of the bits on all carriers. Thereby, one may finally end up in an allocation under increased target rates for the nominal problem which is feasible for DRP in (28) under worst-case parameters. Notably, this approach would not even guarantee the robust optimal solution if we would tune all target rates separately. However, it may serve as a reference on how much we “save” in power by systematic, worst-case optimization. We note that our robust optimization approach has the additional computational advantage of calling robust EEOSB (or any other robust DSM method used for that purpose) only once, while the heuristic search needs to call EEOSB numerous times, depending on the targeted search accuracy. The maximum possible worst-case rate that can be achieved by this search strategy is the worst-case rate for the nominal max-min target rate, cf. Section V-E.

We see that this search strategy demands by far more extra energy compared to our robust DSM approach, cf. Fig. 7. This motivates once more the incorporation of uncertainty into the DSM problem. For the higher target rates, it even becomes infeasible using this heuristic to retain feasibility under parameter uncertainty and integer rounding of worst-case bit allocations. While we note that the heuristic search achieves similar sum-power

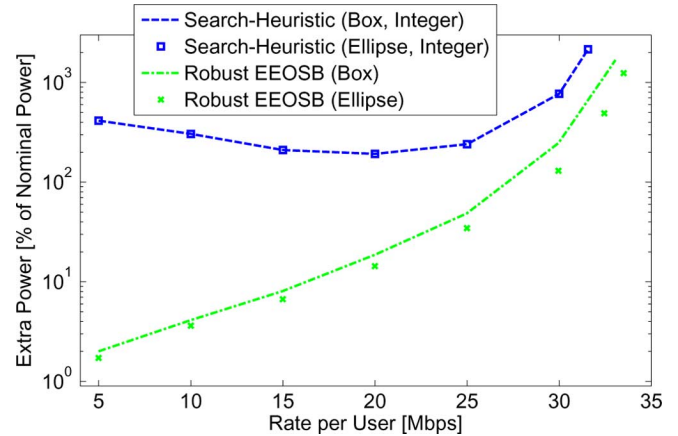


Fig. 7. Extra sum-power of heuristic target-rate search and robust optimization compared to the nominal (nonrobust) sum-power ($\varepsilon = 1$, box/ellipsoid-shaped uncertainty set, integer worst-case bit allocation).

values as robust EEOSB when the rounding procedure to integer worst-case rates is omitted, this comparison would not be fair anymore as robust EEOSB provides an integer worst-case bit allocation.

E. Maximization of Minimum Rates

Differently to all previous investigations on the minimization of the total energy, we now will investigate robust DSM for the maximization of the minimum target rate among users. For this purpose, we enclosed the robust EEOSB algorithm in a bisection loop, searching for the highest feasible minimum target rate equal for all users. In this search the users’ target rates are increased when a feasible solution was found for the previous rates (which are equal for all users), while they are decreased when EEOSB states the problem’s infeasibility, cf. the infeasibility detection mechanism in the original EEOSB algorithm [15]. This process continues until the maximum of the minimum target rate is found up to a certain accuracy.¹

An evaluation of this method is depicted in Fig. 8, where we see a decreasing max-min rate for increasing robustness, i.e., uncertainty parameter ε , see the similarity to Fig. 5. Notably, for $\varepsilon \leq 0.1$ the loss in max-min rate compared to the nominal max-min value is less than 2% (≈ 0.73 Mb/s/user) under box-shaped uncertainty sets and less than 1.5% (≈ 0.55 Mb/s/user) under ellipsoidal uncertainty sets. The largest difference between the two set shapes among the simulated uncertainty values (≈ 0.55 Mb/s) can be seen for a medium-size uncertainty $\varepsilon = 0.5$. In this scenario, the maximum possible loss in max-min rate due to robustness is $\approx 15\%$, cf. $\varepsilon = 10$ in Fig. 8. At this point, the bit allocation is already orthogonal among users and further uncertainty incurs therefore no additional loss in rate, cf. also Section V-B.

VI. CONCLUSION

In this paper, we studied robust dynamic spectrum management (DSM) for minimizing the energy consumption in discrete multitone (DMT) based digital subscriber line (DSL) transceivers. We proposed an application of the robust optimization framework to DMT systems, based on an uncertainty parameter

¹The bisection search was stopped when the search uncertainty dropped below $10^{-3}\%$ of the shown target rates.

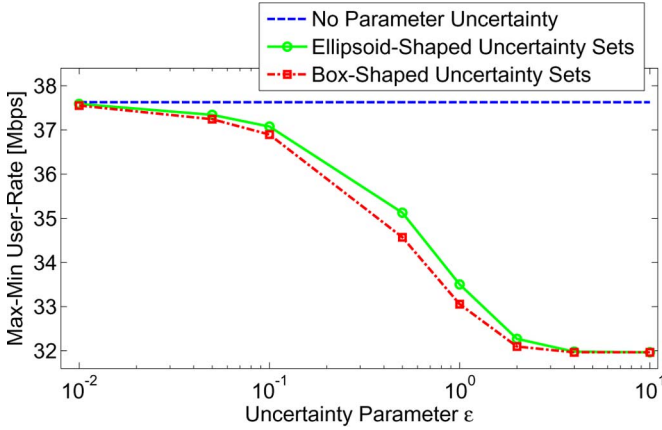


Fig. 8. Dependency of the maximum minimum user rate on uncertainty parameter ϵ in a three-user VDSL scenario.

describing the multiplicative uncertainties in crosstalk noise. Taking these uncertainties explicitly into account ensures feasibility of minimum power allocations in DMT systems under a deterministic crosstalk parameter uncertainty model.

Robust power allocation and the allocation of bits to carriers could be seen to be two separate but interdependent mechanisms. We have further seen that the assumption of normalized crosstalk coefficients lying in ellipsoidal uncertainty sets results in a high computational overhead for a *central* spectrum balancing scheme compared to box-shaped ones, increasing exponentially with the number of users. *Iterative* and less complex DSM algorithms can, however, still be deployed under the robust optimization framework.

Simulation results demonstrate that while box-shaped uncertainty sets are more robust, ellipsoidal ones have a lower cost in terms of power consumption. However, as ellipsoidal uncertainty sets introduce a form of coupling among users one loses the potential of distributed DSM schemes. Furthermore, the difference in sum-power between these two approaches was seen to be small for low/high uncertainties and target rates. This can be explained by the capability of the proposed central and robust DSM scheme to avoid high crosstalk when profitable. Differently, the sum-power difference between the two approaches did not vanish at the higher uncertainties/target rates when an iterative DSM scheme was applied, due to its larger suboptimality and correspondingly smaller rate region.

We also compared our method to a strategy that ensures feasibility of integer bit allocations under parameter uncertainty through heuristically increasing the users' target rates. Supporting our robust optimization approach, this more complex heuristic was seen to necessitate many orders of magnitude more energy compared to our central robust DSM scheme.

Concluding, we believe that box-constrained uncertainty regions (i.e., safety margins on crosstalk coefficients) are the most promising worst-case approach in *practical* DSL systems. Furthermore, they are implementable without changes in current DSM algorithms.

APPENDIX

A. Proof of Proposition 2

The first part of the outage probability bounds can be immediately derived based on [8] as follows. The outage probability

of an allocation \mathbf{p}^c in Problem (21) under symmetric distribution of crosstalk coefficients in the interval (23) can (based on the constraint inequalities in (21)) be written as

$$\sigma = \Pr \left\{ p_u^c - \Gamma \gamma_u^c (\mathbf{p}^c)^T \mathbf{G}_u^c - \varepsilon_u \Gamma \gamma_u^c (\mathbf{p}^c)^T \text{diag}(\mathbf{G}_u^c) \boldsymbol{\xi}_u < n_u^c \right\} \quad (34)$$

where $\boldsymbol{\xi}_u \in \mathcal{R}^U$, with $\xi_{uv} \in [-1, 1]$ being independent, symmetrically distributed random variables following from the definition of the distribution in (23). A solution to (19) is necessarily feasible and we may hence insert the constraints from (19) into (34), giving

$$\sigma \leq \Pr \left\{ \varepsilon_u \Gamma \gamma_u^c \|\text{diag}(\mathbf{G}_u^c) \mathbf{p}^c\|_2 + n_u^c - \varepsilon_u \Gamma \gamma_u^c (\mathbf{p}^c)^T \text{diag}(\mathbf{G}_u^c) \boldsymbol{\xi}_u < n_u^c \right\}, \quad (35)$$

$$= \Pr \left\{ (\mathbf{p}^c)^T \text{diag}(\mathbf{G}_u^c) \boldsymbol{\xi}_u > \|\text{diag}(\mathbf{G}_u^c) \mathbf{p}^c\|_2 \right\}. \quad (36)$$

The result follows together with the probability bound used in the proof to [8, Prop. 3.1]

$$\Pr \left\{ \sum_{v=1}^U a_v \xi_{uv} > \Omega \sqrt{\sum_{v=1}^U a_v^2} \right\} \leq e^{-\Omega^2/2} \quad (37)$$

where $a_v \in \mathcal{R}$, $\Omega \in \mathcal{R}_+$, ξ_{uv} are random variables with properties as specified above, and e is Euler's number.

In the case of uniformly distributed parameters \tilde{G}_{uv}^c we may simply relate the volumes of ellipsoidal [31, p. 67] and box-shaped uncertainty regions from (15) and (20) to obtain the second given outage probability bound. \square

B. Proof of Proposition 3

In the following we will derive feasibility conditions of robust power-allocations for Problem (21) dependent on the matrix $\mathbf{F}^c, c \in \mathcal{C}$, defined in (4) and the multiplicative uncertainty parameters $\boldsymbol{\varepsilon}$. Regarding the feasibility condition in (7), for feasibility of (21) it has to hold that the spectral radius $\rho(\mathbf{F}^c + \Delta \mathbf{F}^{c, \text{box}}) < 1$, where $\Delta \mathbf{F}^{c, \text{box}} \in \mathcal{R}^{U \times U}, \forall c \in \mathcal{C}$,

$$\Delta \mathbf{F}_{uv}^{c, \text{box}} = \Gamma \gamma_u^c \tilde{\eta}_{uv}^c G_{uv}^c = \tilde{\eta}_{uv}^c \mathbf{F}_{uv}^c \leq \varepsilon_u \mathbf{F}_{uv}^c \quad (38)$$

and $\tilde{\eta}_u^c \in \mathcal{R}^U$ is an arbitrary vector with $\tilde{\eta}_{uv}^c \leq \varepsilon_u, \forall u \in \mathcal{U}, c \in \mathcal{C}$, cf. the constraints in (21) and the definitions in (4), (17), and (20). Reformulation of $\rho(\mathbf{F}^c + \Delta \mathbf{F}^{c, \text{box}})$ as follows, where $\|\cdot\|_F$ denotes the Frobenius norm, yields

$$\rho(\mathbf{F}^c + \Delta \mathbf{F}^{c, \text{box}}) \leq \|\mathbf{F}^c + \Delta \mathbf{F}^{c, \text{box}}\|_2 \quad (39a)$$

$$\leq \|\mathbf{F}^c\|_2 + \|\Delta \mathbf{F}^{c, \text{box}}\|_F \quad (39b)$$

$$= \|\mathbf{F}^c\|_2 + \Gamma \sqrt{\sum_{u \in \mathcal{U}} \gamma_u^c \sum_{v \in \mathcal{U}} |G_{uv}^c \tilde{\eta}_{uv}^c|^2} \quad (39c)$$

$$\leq \|\mathbf{F}^c\|_2 + \Gamma \sqrt{\sum_{u \in \mathcal{U}} \gamma_u^c \sum_{v \in \mathcal{U}} |G_{uv}^c|^2 \varepsilon_u^2} \quad (39d)$$

$$= \|\mathbf{F}^c\|_2 + \Gamma \sqrt{\sum_{u \in \mathcal{U}} \varepsilon_u^2 \gamma_u^c \sum_{v \in \mathcal{U}} |G_{uv}^c|^2} \quad (39e)$$

$$\leq \|\mathbf{F}^c\|_2 + \|\mathbf{F}^c\|_F \cdot \|\boldsymbol{\varepsilon}\|_2 \quad (39f)$$

$$\leq \|\mathbf{F}^c\|_2 \cdot \left(1 + \sqrt{U}\|\boldsymbol{\varepsilon}\|_2\right) \quad (39g)$$

where in particular (39c) follows from (38) and the definition of the Frobenius norm, and (39d) follows from the definition of $\tilde{\eta}_u^c$. Hence, $\|\mathbf{F}^c\|_2 \cdot \left(1 + \sqrt{U}\|\boldsymbol{\varepsilon}\|_2\right) < 1$ is sufficient for $\rho(\mathbf{F}^c + \Delta\mathbf{F}^{c,\text{box}}) < 1$ to hold. By (22), this condition is also sufficient for feasibility of (19), which proves the first part of the proposition. Having the same uncertainty parameter ε for all users we can write more simply $\Delta\mathbf{F}^{c,\text{box}} = \varepsilon\mathbf{F}^c$, and as the largest eigenvalue necessarily also scales with $(1 + \varepsilon)$ we obtain the second part of the proposition. \square

C. Proof of Proposition 4

In order to derive a subgradient of the optimum to the dual robust DSM problem (DRP) in (28) with ellipsoidal uncertainty regions, we first interpret the optimal power-allocation $\mathbf{p}^{c,*}$ to subproblem (19) being a function $\mathbf{p}^c(\boldsymbol{\mu}^{c,*})$ of the optimal Lagrange multipliers for the SINR-constraints in (19), cf. (29) and (30). Furthermore, the dual function in (29) with uncertainty parameters $\boldsymbol{\varepsilon}$ can be written as

$$\tilde{g}_\varepsilon^c(\mathbf{b}^c, \boldsymbol{\lambda}, \boldsymbol{\mu}^c) = \min_{\mathbf{p} \succeq \mathbf{0}} \{L_{\text{rob}}^c(\mathbf{p}^c, \mathbf{b}^c, \boldsymbol{\lambda}, \boldsymbol{\mu}^c)\} \quad (40)$$

where $L_{\text{rob}}^c(\mathbf{p}^c, \mathbf{b}^c, \boldsymbol{\lambda}, \boldsymbol{\mu}^c)$ is a linear function in $\boldsymbol{\varepsilon}$, cf. (30). Note that Danskin's theorem [21, p. 737] does not require any additional assumptions on convexity of $\tilde{g}_\varepsilon^c(\mathbf{b}^c, \boldsymbol{\lambda}, \boldsymbol{\mu}^c)$ w.r.t. $\boldsymbol{\mu}^c$ and is therefore applicable to our case, yielding a subgradient $\mathbf{g} \in \mathcal{R}^U$ of $\sum_{c \in \mathcal{C}} \tilde{g}_{\text{rob}}^c(\boldsymbol{\lambda}^*, \mathbf{b}^{c,*})$ in (28) w.r.t. $\boldsymbol{\varepsilon}$ in the form of

$$g_u = \sum_{c \in \mathcal{C}} \mu_u^{c,*} \Gamma \gamma_u^c \|\text{diag}(\mathbf{G}_u^c \mathbf{p}^c(\boldsymbol{\mu}^{c,*}))\|_2, \quad \forall u \in \mathcal{U}. \quad (41)$$

This can also be seen by the following relations. Collecting all terms in (30) for a carrier c excluding the target-rate related terms, we define the power-allocation related function

$$h_c(\tilde{\boldsymbol{\varepsilon}}) = \max_{\boldsymbol{\mu}^c \succeq \mathbf{0}} \left\{ \sum_{u \in \mathcal{U}} \left(w_u p_u^c(\boldsymbol{\mu}^c) + \mu_u^c \left(\Gamma \gamma_u^c (\mathbf{p}^c)^T (\boldsymbol{\mu}^c) \mathbf{G}_u^c - p_u^c(\boldsymbol{\mu}^c) + \tilde{\varepsilon}_u \Gamma \gamma_u^c \|\text{diag}(\mathbf{G}_u^c \mathbf{p}^c(\boldsymbol{\mu}^c))\|_2 + n_u^c \right) \right) \right\}. \quad (42)$$

Then we have that

$$\begin{aligned} h_c(\tilde{\boldsymbol{\varepsilon}}) &\geq \sum_{u \in \mathcal{U}} \left(w_u p_u^c(\boldsymbol{\mu}^{c,*}) + \mu_u^{c,*} \left(\Gamma \gamma_u^c (\mathbf{p}^c)^T (\boldsymbol{\mu}^{c,*}) \mathbf{G}_u^c - p_u^c(\boldsymbol{\mu}^{c,*}) \right. \right. \\ &\quad \left. \left. + \tilde{\varepsilon}_u \Gamma \gamma_u^c \|\text{diag}(\mathbf{G}_u^c \mathbf{p}^c(\boldsymbol{\mu}^{c,*}))\|_2 + n_u^c \right) \right) \\ &= h_c(\boldsymbol{\varepsilon}) + (\tilde{\boldsymbol{\varepsilon}} - \boldsymbol{\varepsilon})^T [\mu_u^{c,*} \Gamma \gamma_u^c \|\text{diag}(\mathbf{G}_u^c \mathbf{p}^c(\boldsymbol{\mu}^{c,*}))\|_2]_{u=1}^U \end{aligned} \quad (43)$$

$$(44)$$

where the first inequality holds since $\boldsymbol{\mu}^{c,*}$ is the maximizing value in (42) for $h_c(\boldsymbol{\varepsilon})$ and not necessarily for $h_c(\tilde{\boldsymbol{\varepsilon}})$, and $[\cdot]_{u=1}^U \in \mathcal{R}^U$ denotes the vector made up by the given elements indexed by u . Equation (44) is however exactly the definition of a subgradient [21, p. 731]. As the subgradient of a sum equals the sum of subgradients, the result given in (41) follows. We note that the subgradient will not be unique in general as the per-carrier subproblems are coupled by the target-rate

constraints, and $\mathbf{p}^c(\boldsymbol{\mu}^{c,*})$ is obviously discontinuous as we vary $\boldsymbol{\varepsilon}$ when the optimal, *discrete* bit-allocation \mathbf{b}^* changes, cf. also [10, Sec. 5.6.3]. Furthermore, it is this discreteness of \mathbf{b} which hinders us to differentiate $L_{\text{rob}}^c(\mathbf{p}^c, \mathbf{b}^c, \boldsymbol{\lambda}, \boldsymbol{\mu}^c)$ w.r.t. b_u^c in order to denote \mathbf{g} solely depending on $\boldsymbol{\lambda}$. \square

Proof of Proposition 5: We begin by proofing the first part of the proposition stated in relation (32). Its necessity follows from the feasibility of the solution $\mathbf{p}^{c,*}$ to Problem (19) (or (21), respectively) for the power-allocation subproblem (19) (or (21), respectively). To show sufficiency, assume that $\exists u \in \mathcal{U} : p_u^{c,*} > \bar{p}_u^c$, $\bar{\mathbf{p}}^c$ denoting the users' spectral mask constraints on carrier c , and that there exists a feasible allocation $\mathbf{p} \preceq \bar{\mathbf{p}}^c$ fulfilling the constraints in (19) (or (21), respectively) with *strict* inequality. Then we could decrease the power-allocation of those users exceeding their SINR-target, staying below the mask constraints. At the same time the other users' SINR constraints would stay feasible as the left-hand-side of the constraints in (19) (or (21), respectively) are monotonously decreasing functions of other users' powers. Following this way we end up in an allocation $\tilde{\mathbf{p}} \preceq \bar{\mathbf{p}}^c$ fulfilling the SINR constraints with equality. In Section III we stated that at the unique solution to (3) all SINR-constraints are tight. The same arguments can be applied to show corresponding statements for the solutions of robust power-allocation subproblems (19) and (21), respectively. Using this uniqueness property, it follows that $\tilde{\mathbf{p}} = \mathbf{p}^{c,*} \preceq \bar{\mathbf{p}}^c$, which contradicts the assumption $\exists u \in \mathcal{U} : p_u^{c,*} > \bar{p}_u^c$ and concludes the proof of (32).

To proof the final statement in the proposition, we note that $\mathcal{P}^{c,\text{nom}} \supseteq \mathcal{P}^{c,\text{ell}} \supseteq \mathcal{P}^{c,\text{box}}$, where $\mathcal{P}^{c,\text{nom}}$, $\mathcal{P}^{c,\text{ell}}$ and $\mathcal{P}^{c,\text{box}}$ are the feasible sets in problems (3), (19) and (21), respectively. Assuming (unique) solutions $\hat{\mathbf{p}}^{c,*}$, $\check{\mathbf{p}}^{c,*}$ and $\tilde{\mathbf{p}}^{c,*}$ to nominal problem (3) and robust problems (19) and (21) exist, it trivially holds that

$$\exists \mathbf{p}^c \in \mathcal{P}^{c,\text{ell}} : \mathbf{p}^c \preceq \check{\mathbf{p}}^{c,*} \quad (45)$$

$$\exists \mathbf{p}^c \in \mathcal{P}^{c,\text{box}} : \mathbf{p}^c \preceq \tilde{\mathbf{p}}^{c,*}. \quad (46)$$

Using $\mathcal{P}^{c,\text{nom}} \supseteq \mathcal{P}^{c,\text{ell}} \supseteq \mathcal{P}^{c,\text{box}}$ we also have

$$\exists \mathbf{p}^c \in \mathcal{P}^{c,\text{nom}} : \mathbf{p}^c \preceq \check{\mathbf{p}}^{c,*}, \quad (47)$$

$$\exists \mathbf{p}^c \in \mathcal{P}^{c,\text{ell}} : \mathbf{p}^c \preceq \tilde{\mathbf{p}}^{c,*}, \quad (48)$$

and using relation (32) it follows that

$$\nexists u \in \mathcal{U} : \hat{p}_u^{c,*} > \check{p}_u^{c,*} \quad (49)$$

$$\nexists u \in \mathcal{U} : \check{p}_u^{c,*} > \tilde{p}_u^{c,*} \quad (50)$$

which concludes the proof. \square

ACKNOWLEDGMENT

The authors would like to thank J. Jaldén for improving this manuscript by his invaluable comments.

REFERENCES

- [1] "Power Saving Tutorials," ITU-T Study Group 15, Tutorials and Presentations, Geneva, Switzerland, 2008 [Online]. Available: <http://www.itu.int/ITU-T/studygroups/com15/tutorials/power.html>
- [2] "Code of conduct on energy consumption of broadband equipment," European Commission, Directorate-General JRC; Institute for the Environment and Sustainability; Renewable Energies Unit, Tech. Rep. (V1 Jul. 2006) V2, 2007.

- [3] M. Wolkerstorfer, D. Statovci, and T. Nordström, "Dynamic spectrum management for energy-efficient transmission in DSL," in *Proc. IEEE Int. Conf. Communications Systems 2008 (ICCS)*, Guangzhou, China, Nov. 19–21, 2008, pp. 1015–1020.
- [4] J. Cioffi, H. Zou, A. Chowdhery, W. Lee, and S. Jagannathan, "Greener copper with dynamic spectrum management," in *Proc. IEEE Global Telecommunications Conf. 2008 (IEEE GLOBECOM)*, New Orleans, LA, Nov. 30–Dec. 4, 2008, pp. 1–5.
- [5] P. Tsiaflakis, Y. Yi, M. Chiang, and M. Moonen, "Green DSL: Energy-efficient DSM," presented at the IEEE Int. Conf. Communications 2009 (ICC), Dresden, Germany, Jun. 14–18, 2009.
- [6] S. Jagannathan, C. S. Hwang, and J. M. Cioffi, "Margin optimization in digital subscriber lines employing level-2 dynamic spectrum management," in *Proc. IEEE Int. Conf. Commun. 2008 (ICC)*, Beijing, China, May 19–23, 2008, pp. 435–440.
- [7] J. Verlinden and D. V. Bruyssel, "Virtual noise mechanism," in *ANSI Contribution*, San Francisco, CA, Feb. 2005, NIPP-NAI-2005-049.
- [8] A. Ben-Tal and A. Nemirovski, "Robust solutions of linear programming problems contaminated with uncertain data," *Math. Program.*, vol. 88, pp. 411–424, 2000.
- [9] D. Bertsimas and M. Sim, "The price of robustness," *Oper. Res.*, vol. 52, no. 1, pp. 35–53, 2004.
- [10] S. Boyd and L. Vandenberghe, *Convex Optimization*. Cambridge, U.K.: Cambridge Univ. Press, 2004.
- [11] A. Pascual-Iserte, D. Palomar, A. Perez-Neira, and M. Lagunas, "A robust maximin approach for MIMO communications with imperfect channel state information based on convex optimization," *IEEE Trans. Signal Process.*, vol. 54, no. 1, pp. 346–360, Jan. 2006.
- [12] R. Lorenz and S. Boyd, "Robust minimum variance beamforming," *IEEE Trans. Signal Process.*, vol. 53, no. 5, pp. 1684–1696, May 2005.
- [13] K. Yang, Y. Wu, J. Huang, X. Wang, and S. Verdu, "Distributed robust optimization for communication networks," in *Proc. IEEE Int. Conf. Computer Communications (INFOCOM)*, Phoenix, AZ, Apr. 15–17, 2008, pp. 1157–1165.
- [14] S. Kandukuri and S. Boyd, "Optimal power control in interference limited fading wireless channels with outage probability specifications," *IEEE J. Wireless Commun.*, vol. 1, no. 1, pp. 46–55, Jan. 2002.
- [15] M. Wolkerstorfer, T. Nordström, and D. Statovci, "Energy-efficient balancing in DSL," in *Eur. Signal Processing Conf. (EU-SIPCO)*, Aalborg, Denmark, Aug. 23–27, 2010.
- [16] R. Cendrillon, W. Yu, M. Moonen, J. Verlinden, and T. Bostoen, "Optimal multiuser spectrum balancing for digital subscriber lines," *IEEE Trans. Commun.*, vol. 54, pp. 922–933, May 2006.
- [17] Y. Yu and G. B. Giannakis, "Joint congestion control and OFDMA scheduling for hybrid wireline-wireless networks," in *Proc. IEEE Int. Conf. Proc. Computer Commun. (INFOCOM)*, Anchorage, AL, May 6–12, 2007, pp. 973–981.
- [18] G. J. Foschini and Z. Miljanic, "A simple distributed autonomous power control algorithm and its convergence," *IEEE Trans. Veh. Technol.*, vol. 42, pp. 641–646, Nov. 1993.
- [19] M. Chiang, P. Hande, T. Lan, and C. W. Tan, *Power Control Wireless Cellular Netw.*, vol. 2, no. 4, Jul. 2008.
- [20] R. D. Yates, "A framework for uplink power control in cellular radio systems," *IEEE J. Sel. Areas Commun.*, vol. 13, pp. 1341–1347, Sep. 1995.
- [21] D. P. Bertsekas, *Nonlinear Programming*. Singapore: Athena Scientific, 1999.
- [22] A. Ghosh and S. Boyd, "Minimax and convex-concave game," in lecture notes for course EE392o: "Optimization Projects" Stanford Univ., Stanford, CA, 2003.
- [23] M. Lobo, L. Vandenberghe, S. Boyd, and H. Lebret, "Applications of second-order cone programming," *Linear Algebra Its Appl.*, vol. 284, pp. 193–228, Nov. 1998.
- [24] *The MOSEK Optimization Toolbox for MATLAB Manual, Version 5.0 (Revision 137)*. Copenhagen, Denmark: MOSEK ApS, 2009.
- [25] C. W. Tan, D. P. Palomar, and M. Chiang, "Energy-robustness tradeoff in cellular network power control," *IEEE/ACM Trans. Netw.*, vol. 17, pp. 912–925, Jun. 2009.
- [26] R. Madan, S. Cui, S. Lall, and A. Goldsmith, "Cross-layer design for lifetime maximization in interference-limited wireless sensor networks," *IEEE Trans. Wireless Commun.*, vol. 5, pp. 3142–3152, Nov. 2006.
- [27] J.-W. Lee, M. Chiang, and A. R. Calderbank, "Price-based distributed algorithms for rate-reliability tradeoff in network utility maximization," *IEEE J. Sel. Areas Commun.*, vol. 24, pp. 962–976, May 2006.
- [28] J. Lee, R. Sonalkar, and J. Cioffi, "Multi-user discrete bit-loading for DMT-based DSL systems," in *Proc. IEEE Global Telecommun. Conf. 2002 (IEEE GLOBECOM)*, Taipei, Taiwan, China, Nov. 17–21, 2002, vol. 2, pp. 1259–1263.
- [29] "Transmission and Multiplexing (TM); Access Transmission Systems on Metallic Access Cables; Very High Speed Digital Subscriber Line (VDSL); Part 1: Functional Requirements," ETSI, Tech. Rep. TM6 TS 101 270-1, Version 1.3.1, 2003.
- [30] F. Lindqvist *et al.*, "Crosstalk channel estimation via standardized two-port measurements," *EURASIP J. Adv. Signal Process.*, vol. 2008, Dec. 2008, 14 pp., doi: 10.1155/2008/916865.
- [31] M. Grötschel, L. Lovász, and A. Schrijver, *Geometric Algorithms and Combinatorial Optimization*, ser. Algorithms and Combinatorics, 2nd ed. New York: Springer, 1993, vol. 2.



Martin Wolkerstorfer (S'09) was born in Helfenberg, Austria, in 1982. He received the Dipl.Ing. degree (Master's degree equivalent) in electrical engineering from Graz University of Technology, Austria, in 2007. He is currently working towards the Ph.D. degree at the Telecommunications Research Center Vienna (FTW).

His research interests include the application of optimization theory in signal processing, energy-efficient communication systems, and cross-layer resource allocation in broadband access networks.



Driton Statovci (S'03–M'06) was born in Batllavë, Kosova, in 1972. He received the Inxh.Dipl. degree (Master's degree equivalent) from the Faculty of Electrical Engineering, University of Prishtina, Kosova, in 1996 and the Ph.D. degree from the Vienna University of Technology, Austria, in 2005.

During 2000 and 2002, he was with Ericsson Ahead Communications Systems, Vienna, Austria, where he worked in system design for the transmission of data and voice over DSL access networks. In February 2002, he joined the Telecommunications

Research Center Vienna (FTW), Austria, where he is currently working as a Senior Researcher and Project Manager. Since 2006, he has been working as a Guest Lecturer at the Faculty of Electrical Engineering, University of Prishtina, Kosova. His current research interests include multiuser transmission theory, multicarrier modulation, interference mitigation and cancellation, the application of convex and nonconvex optimization techniques in communication systems, and energy-efficient system design and operation.



Tomas Nordström (S'88–A'95–M'00–SM'01) was born in Härnösand, Sweden, in 1963. He received the M.S.E.E. degree in 1988, the Licentiate degree in 1991, and the Ph.D. degree in 1995, all from the Luleå University of Technology, Sweden.

During 1995 and 1996, he was an Assistant Professor at Luleå University of Technology researching computer architectures, neural networks, and signal processing. Between 1996 and 1999, he was with Telia Research (the research branch of the Swedish incumbent telephone operator), where he

developed broadband Internet communication over twisted copper pairs. He was instrumental in the development of the Zipper-VDSL concept (contributed to the standardization of VDSL in ETSI, ANSI, and ITU) and in the design of the Zipper-VDSL prototype modems. In December 1999, he joined the Telecommunications Research Center Vienna (FTW), where he is a Key Researcher and Project Manager leading the Broadband Wireline Access group. At FTW, he has worked with various aspects of wireline communications like simulation of xDSL systems, cable characterization, RFI suppression, exploiting the common-mode signal in xDSL, and dynamic spectrum management. Since 2009, he has also been an Associate Professor in Computer Systems Engineering at Halmstad University, Sweden. His current research interests include all aspects of energy efficient communication systems, from cross-layer design and signal processing all the way to novel power amplifier designs and multicore computing.